# Iron-mediated aggregation and toxicity in a novel neuronal cell culture model with inducible alpha-synuclein expression

**Martin Bartels[1,2], Daniel Weckbecker[3], Peer-Hendrik Kuhn[4], Sergey Ryazanov[5,6], Andrei Leonov[3,5,6], Christian Griesinger[5,6], Stefan F. Lichtenthaler[7,8], Kai Bötzel[2] and Armin Giese[1*]**

From the [1]Center for Neuropathology and Prion Research, Ludwig-Maximilians-University, Munich, Germany; [2]Department of Neurology, Klinikum der Universität München, Munich, Germany; [3]MODAG GmbH, Wendelsheim, Germany; [4]Institute of Pathology, TUM School of Medicine, Technical University of Munich, Munich, Germany; [5]Center for Nanoscale Microscopy and Molecular Physiology of the Brain, Georg-August-University Göttingen, 37073 Göttingen, Germany; [6]Department of NMR-based Structural Biology, Max Planck Institute for Biophysical Chemistry, 37077 Göttingen, Germany; [7]German Center for Neurodegenerative Diseases (DZNE), and Munich Cluster for Systems Neurology (SyNergy), Munich, Germany; [8]Neuroproteomics, School of Medicine, Klinikum rechts der Isar, and Institute for Advanced Science, Technical University of Munich, 81675 Munich, Germany

[*]To whom correspondence should be addressed: Armin Giese, Center for Neuropathology and Prion Research, Ludwig-Maximilians-University, Munich, Germany, armin.giese@med.uni-muenchen.de; Tel. 0049 89 2180 78007; Fax. 0049 89 2180 78037

**Supplements**

**Supplementary Table 1: List of plasmids**

Information on plasmids used in this study.

| ID | Insert | Backbone |
|---|---|---|
| #1 | V1S | pCS2 |
| #2 | SV2 | pCS2 |
| #3 | SV | pCS2 |
| #4 | Venus | pCS2 |
| #32 | SV2 | F2P-Delta Zeo-LoxP-Ko.Puro-LoxP-STNST-GW(DEST) (636) |
| #33 | V1S | F2P-Delta Zeo-LoxP-Ko.Puro-LoxP-STNST-GW(DEST) (636) |
| #35 | SV | F2P-Delta Zeo-LoxP-Ko.Puro-LoxP-STNST-GW(DEST) (636) |
| #36 | αSyn | F2P-Delta Zeo-LoxP-Ko.Puro-LoxP-STNST-GW(DEST) (636) |
| #37 | Venus | F2P-Delta Zeo-LoxP-Ko.Puro-LoxP-STNST-GW(DEST) (636) |
| #39 | V1S | F2-Delta Zeo-Kozak-Puro-5XUAS-E1b-(GW)Dest (597) |
| #41 | SV | F2-Delta Zeo-Kozak-Puro-5XUAS-E1b-(GW)Dest (597) |
| #42 | αSyn | F2-Delta Zeo-Kozak-Puro-5XUAS-E1b-(GW)Dest (597) |
| #43 | Venus | F2-Delta Zeo-Kozak-Puro-5XUAS-E1b-(GW)Dest (597) |
| #44 | ccdB | F2-Delta Zeo-Kozak-Hygro-5XUAS-E1b-(GW)Dest |
| #45 | ccdB | F2-Delta Zeo-Kozak-Zeo-5XUAS-E1b-(GW)Dest |
| #46 | SV2 in 44 | F2-Delta Zeo-Kozak-Hygro-5XUAS-E1b-(GW)Dest |
| #71 | V1S | P12-HA-TGFa-FLAG |
| #75 | SV2 | P12-HA-TGFa-FLAG |
| #87 | mCherry-NLS | pmCherry-C1 |
| #92 | ccdB | F-Delta Zeo-Kozak-mCherry-NLS-5X UAS-E1b-(GW)Dest |
| #97 | psPAX2 | |
| #98 | VSV-G | pcDNA3.1 |
| #99 | Zeo-GAL4-VP16 | FUGW |
| #100 | Zeo-GAL4-VP16-EcR | FUGW |
| #102 | F2U-Delta Zeo-iCre_ER$^{T2}$ | FUGW |
| #120 | S | F-Delta Zeo-Kozak-mCherry-NLS-5X UAS-E1b-(GW)Dest |
| 597 | ccdB | F2-Delta Zeo-Kozak-Puro-5XUAS-E1b-(GW)Dest |
| 636 | ccdB | F2P-Delta Zeo-LoxP-Ko.Puro-LoxP-STNST-GW(DEST) (636) |
| --- | Empty | pCR8/GW/TOPO+pCS2-MCS |

**Supplementary Table 2: List of primers**

Information on primers used for molecular cloning in this study.

| Primer Name | Sequence (5'-3') |
| --- | --- |
| MB3_SV2_Hind3_f | GATCAAGCTTGCCACCATGGATGTATTCATGAAAGG |
| MB6_V1S_Not1_r | GATCGCGGCCGCTTAGGCTTCAGGTTCGTAG |
| MB8_SV_Hind3_f | GCGCAAGCTTGCCACCATGGATGTATTCATGAAAGG |
| MB9_SV_PspOMI_r | GATCGGGCCCTCTACAAATGTGGTATGGCTG |
| MB10_V_Hind3_f | GATAAAGCTTGCCACCATGGTGAGCAAGGGCGAGG |
| MB11_Syn_Not1_r | GATCGCGGCCGCCTAGGCTTCAGGTTCGTAGTCTTG |
| MB24_V1_HindIIIf | GATCAAGCTTGCCACCATGGTGAGCAAGGGCGAGGAGC |
| MB25_V2_NotI_r | GATCGCGGCCGCTTACTTGTACAGCTCG |
| 42MB_SalI_mCherry_f | GATCGTCGACGCCACCATGGTGAGC |
| 43MB_NsiI_mCherry_r | GATCATGCATTTATCTAGATCCGGTGGATCC |

**Supplementary Table 3: List of viruses**

Plasmids used for production of infectious but replication-incompetent viruses. Co-transfection of HEK293T cells with viruses #97 and #98 and an expression plasmid resulted in production of viruses shown in the right column.

| Plasmid ID | Kind of Plasmid | Insert | Comment | Virus ID |
|---|---|---|---|---|
| #97 | Packaging | psPAX2 | Encodes for viral enzymes gag-pol to generate lentiviruses | |
| #98 | Packaging | VSV-G | Encodes for the envelope glycoprotein VSV-G from Vesicular Stomatitis Virus (broad tropism) | |
| #99 | Expression | Zeo-GAL4-VP16 | Constitutive GAL4 driver | V99 |
| #100 | Expression | Zeo-GAL4-VP16-EcR | Inducible GAL4_EcR driver (+tebufenozide) | V100 |
| #102 | Expression | F2U-Delta Zeo-iCre_ER$^{T2}$ | Inducible Cre_ER$^{T2}$ driver (+4-OH-tamoxifen) | V102 |
| #32 | Expression | SV2 | Cre-loxP receiver (puromycin resistance) | V32 |
| #33 | Expression | V1S | Cre-loxP receiver (puromycin resistance) | V33 |
| #34 | Expression | V1 | Cre-loxP receiver (puromycin resistance) | V34 |
| #35 | Expression | SV | Cre-loxP receiver (puromycin resistance) | V35 |
| #36 | Expression | S | Cre-loxP receiver (puromycin resistance) | V36 |
| #37 | Expression | V | Cre-loxP receiver (puromycin resistance) | V37 |
| #39 | Expression | V1S | GAL4-UAS receiver (puromycin resistance) | V39 |
| #41 | Expression | SV | GAL4-UAS receiver (puromycin resistance) | V41 |
| #42 | Expression | S | GAL4-UAS receiver (puromycin resistance) | V42 |
| #43 | Expression | V | GAL4-UAS receiver (puromycin resistance) | V43 |
| #46 | Expression | SV2 | GAL4-UAS receiver (hygromycin resistance) | V46 |
| #120 | Expression | S | GAL4-UAS receiver (mCherry-NLS) | V120 |
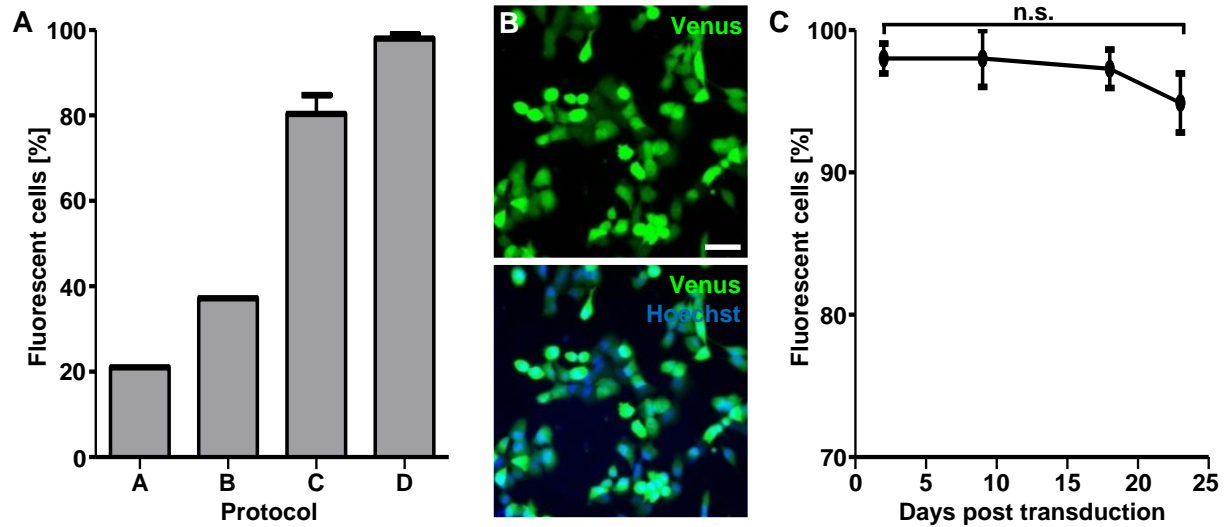
**Supplementary Figure 1.** Stable and highly efficient transduction of H4 cells following protocol D. H4 cells were transduced with the constitutive GAL4 driver virus (V99) and the UAS-SV receiver virus (V41) according to protocols A-D. (A) Quantification of the fraction of Venus-positive cells. (B) Representative images obtained for protocol D. Nuclei were stained with Hoechst33342. Scale bar is 100 μm and valid for both panels. (C) The fraction of positive cells was not significantly changed for 23 days after transduction (Fisher's exact test, n.s.: $p>0.05$). Data points represent mean of 3 to 4 wells; error bars show SEM; at least 300 cells were counted.
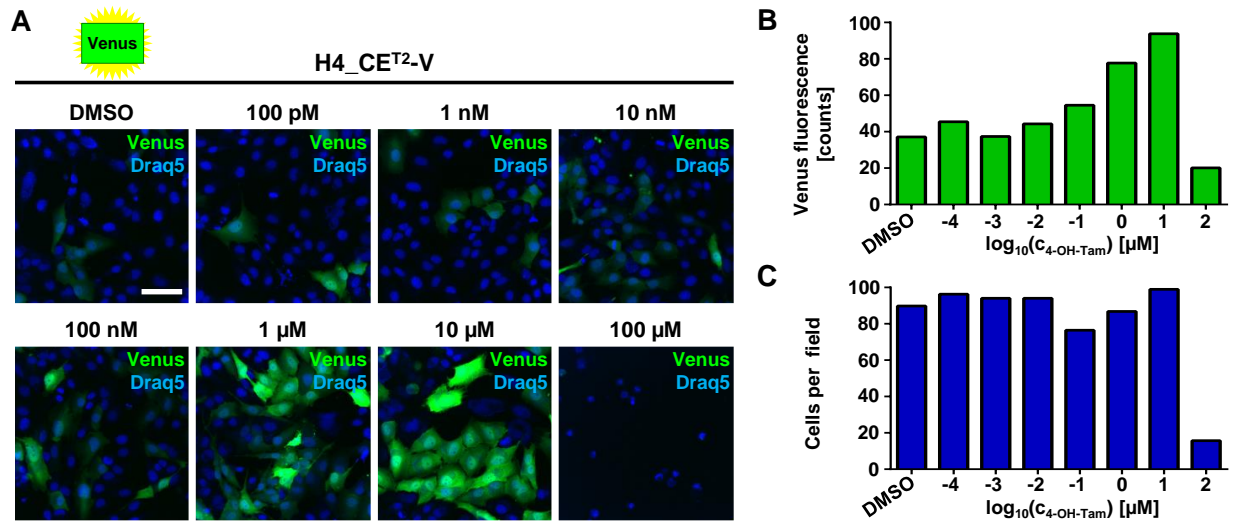
**Supplementary Figure 2.** Maximum transgene induction in H4_CE$^{T2}$-V cells was achieved by 10 μM 4-OH-tamoxifen. H4_CE$^{T2}$-V cells were incubated with different concentrations of 4-OH-tamoxifen ranging from 100 pM to 100 μM or DMSO as control for 72 h to determine its optimal concentration. (A) Fluorescence images showed increasing fluorescence with increasing concentration of 4-OH-tamoxifen up to a concentration of 10 μM. Nuclei were stained with Draq5. Scale bar is 100 μm and valid for all panels. (B) Quantification of fluorescence intensity using the Opera$^®$ system. A maximum in fluorescence intensity was observed upon incubation with 10 μM 4-OH-tamoxifen. Bars in B and C show mean of four wells. (C) Quantification of cell number using the Opera$^®$ system. Incubation with 100 μM 4-OH-tamoxifen led to decreased cell number whereas all other concentrations showed no adverse effect on cell number.
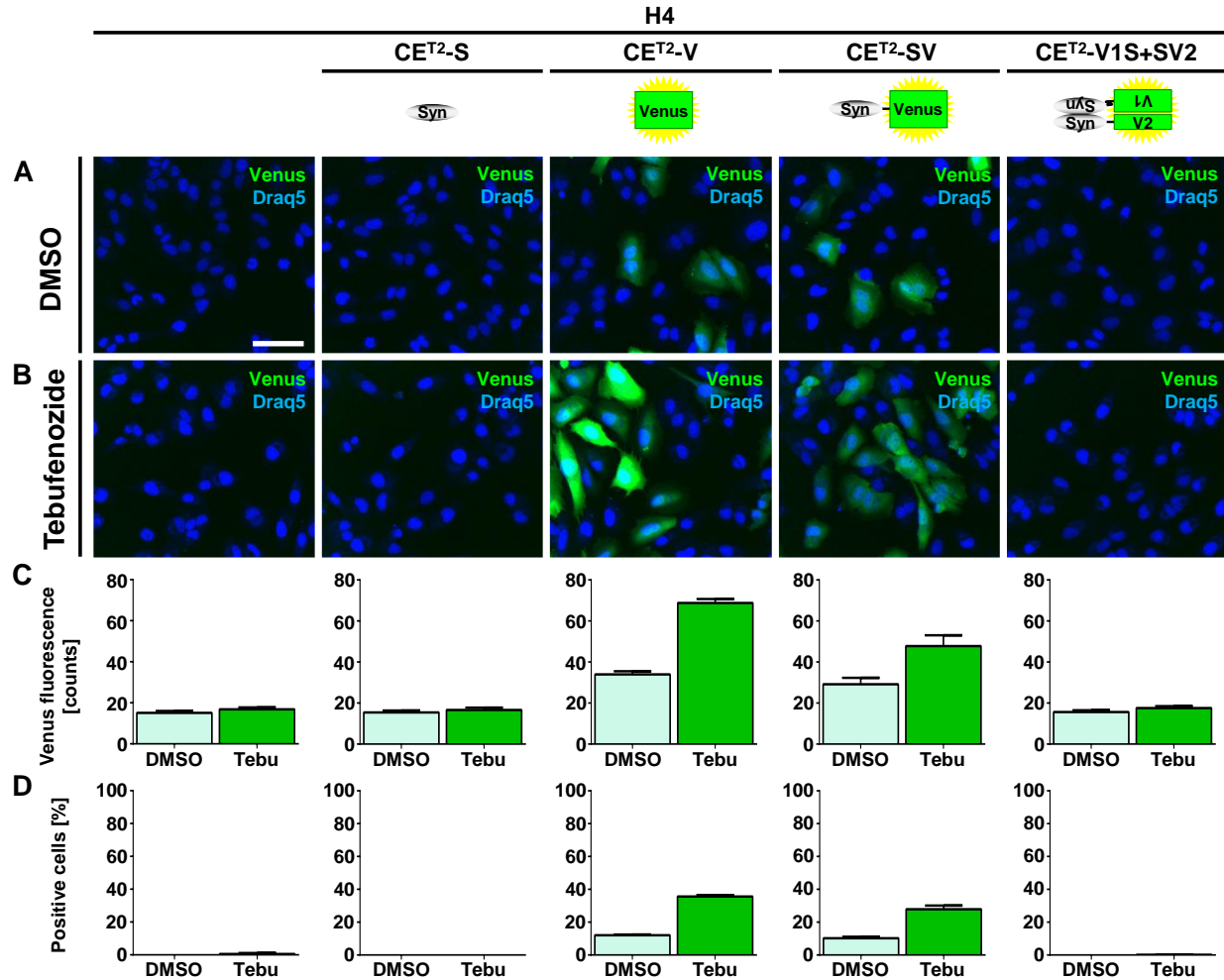
**Supplementary Figure 3.** Induction of transgene expression in H4_CE^(T2) cells. The generated H4_CE^(T2) cell lines were incubated with 0.1% DMSO or 10 μM 4-OH-tamoxifen for 48 h. (A) Representative fluorescence images of cells incubated with 0.1% DMSO. Nuclei were stained with Draq5. Scale bar is 100 μm and valid for all panels in A and B. (B) Representative fluorescence images of cells incubated with 10 μM 4-OH-tamoxifen. (C) Quantification of the mean cellular Venus fluorescence intensity of H4 cells upon incubation with DMSO or 4-OH-tamoxifen using the Acapella® software. Bars in C ans D show mean of 3 independent experiments; error bars show SEM; Tam: 4-OH-tamoxifen. (D) Quantification of the fraction of Venus-positive H4 cells upon incubation with DMSO or 4-OH-tamoxifen using the Acapella® software. Quantification was performed by setting an arbitrary threshold for Venus fluorescence intensity.
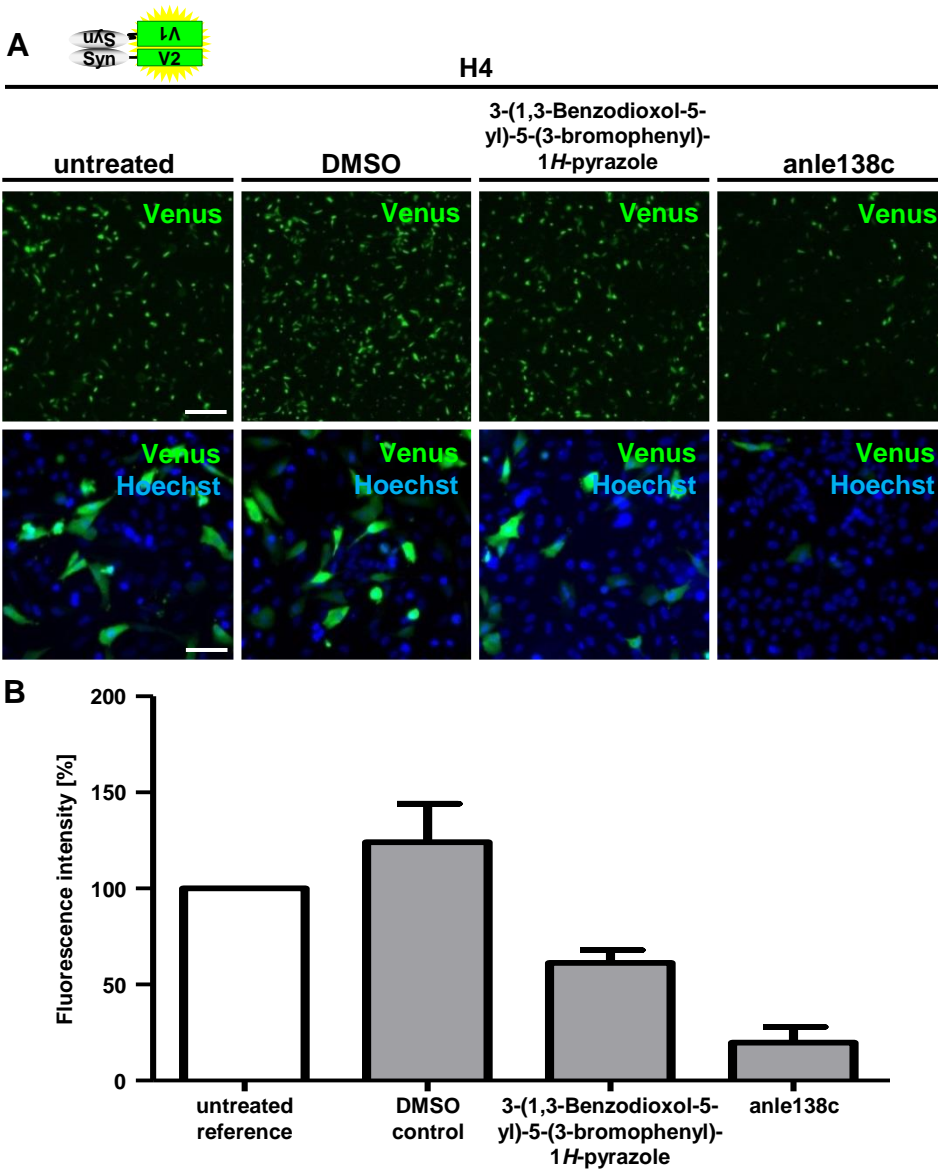
**Supplementary Figure 4.** Reduced fluorescence intensity in the BiFC system as result of aggregation inhibitors. H4 cells were transiently transfected with the BiFC plasmids and left untreated or were incubated with DMSO (control), 3-(1,3-Benzodioxol-5-yl)-5-(3-bromophenyl)-1*H*-pyrazole, anle138c, or baicalein. (A) Fluorescence images showed a decrease in fluorescence intensity upon treatment with 3-(1,3-Benzodioxol-5-yl)-5-(3-bromophenyl)-1*H*-pyrazole, anle138c, and baicalein compared to treatment with DMSO. Nuclei were stained with Hoechst33342. Scale bar in top left panel is 500 μm and valid for images in the first row. Scale bar in the left panel of the second row is 100 μm and valid for images in the second and third row. (B) Cell lysates were analyzed using single particle spectroscopy. Total fluorescence intensity was increased in DMSO-treated cells compared to untreated cells. Fluorescence intensity was decreased upon treatment with 3-(1,3-Benzodioxol-5-yl)-5-(3-bromophenyl)-1*H*-pyrazole or anle138c. Bars show mean of 2 individual experiments, error bars show SEM.
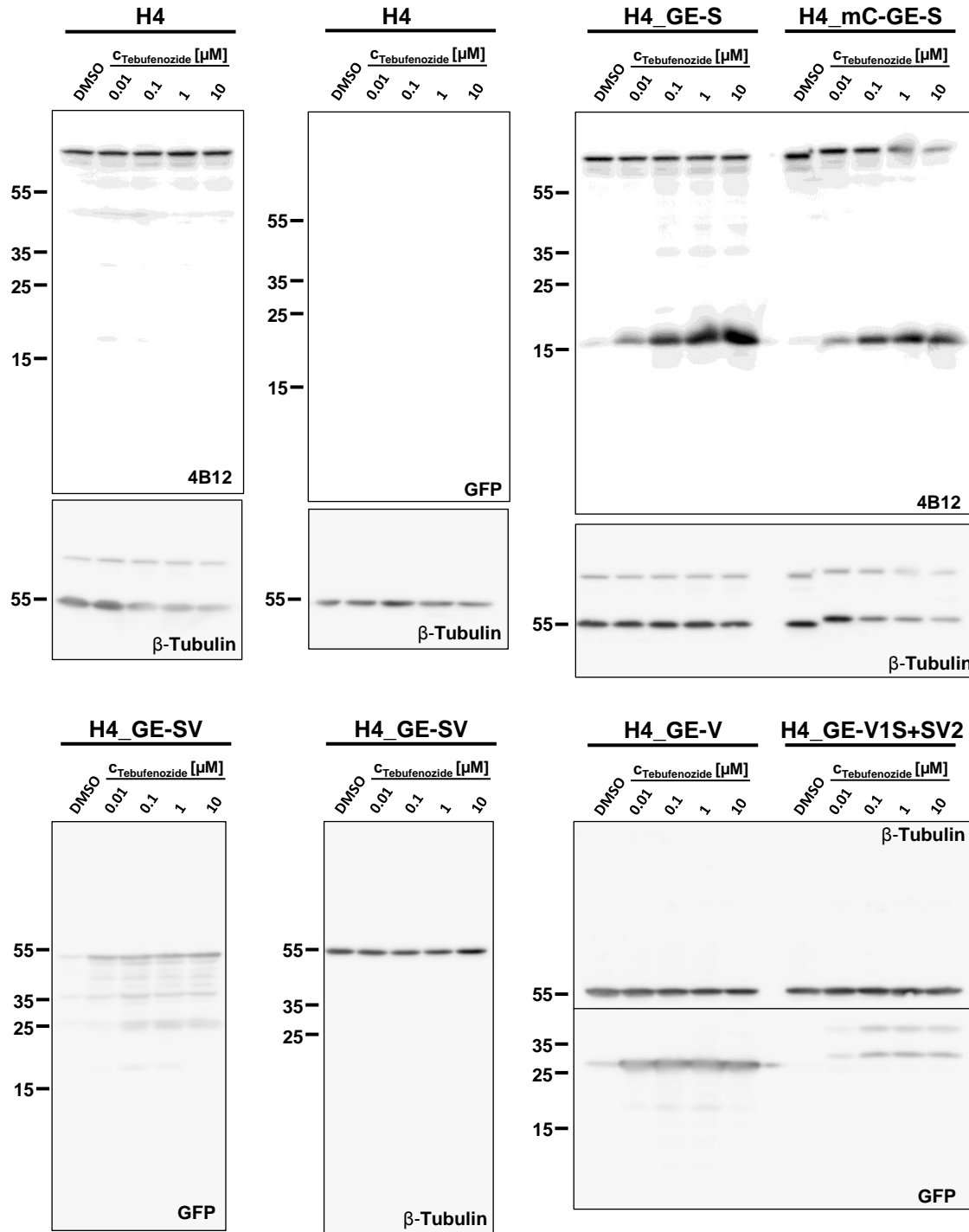
**Supplementary Figure 5.** Full length Western blots corresponding to the panels shown in Figure 4. For details see legend of Figure 4. Blots from H4, H4_GE-S, and H4_mC-GE-S were stripped after incubated with 4B12 or GFP antibody and afterwards incubated with β-Tubulin antibody. For H4_GE-SV, housekeeper was detected on a separate blot. For H4_GE-V and H4_GE-V1S+SV2 the blot was cut at 40 kDa and incubated with β-Tubulin or GFP antibody, respectively.
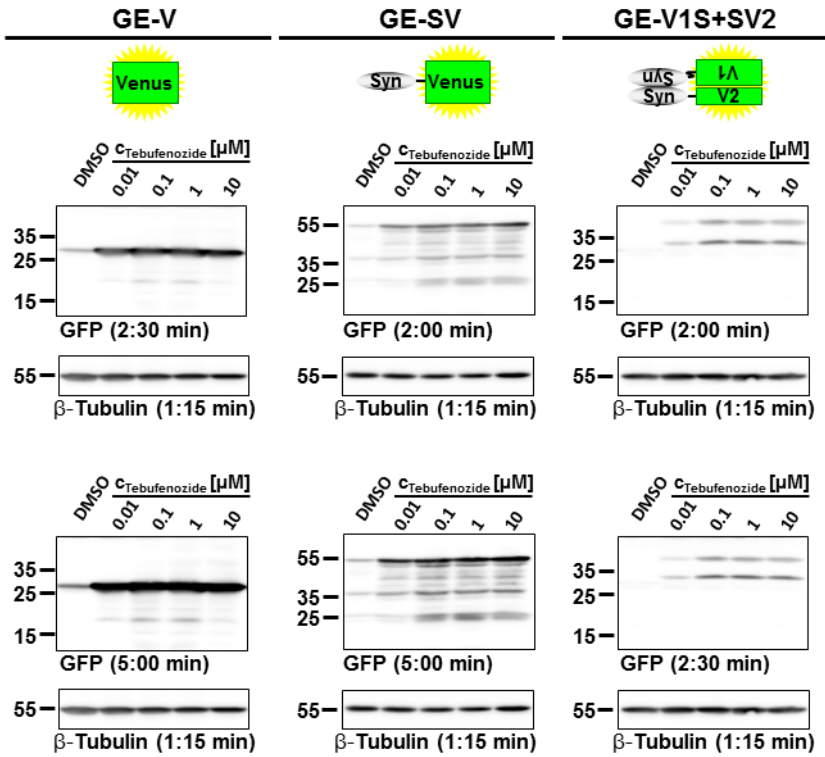
**Supplementary Figure 6.** Additional exposures of Western blots shown in Figure 4. For details see legend of Figure 4. For H4_GE-SV, housekeeper β-Tubulin was detected on a separate blot. For H4_GE-V and H4_GE-V1S+SV2 the blot was cut at 40 kDa and incubated with β-Tubulin or GFP antibody, respectively.
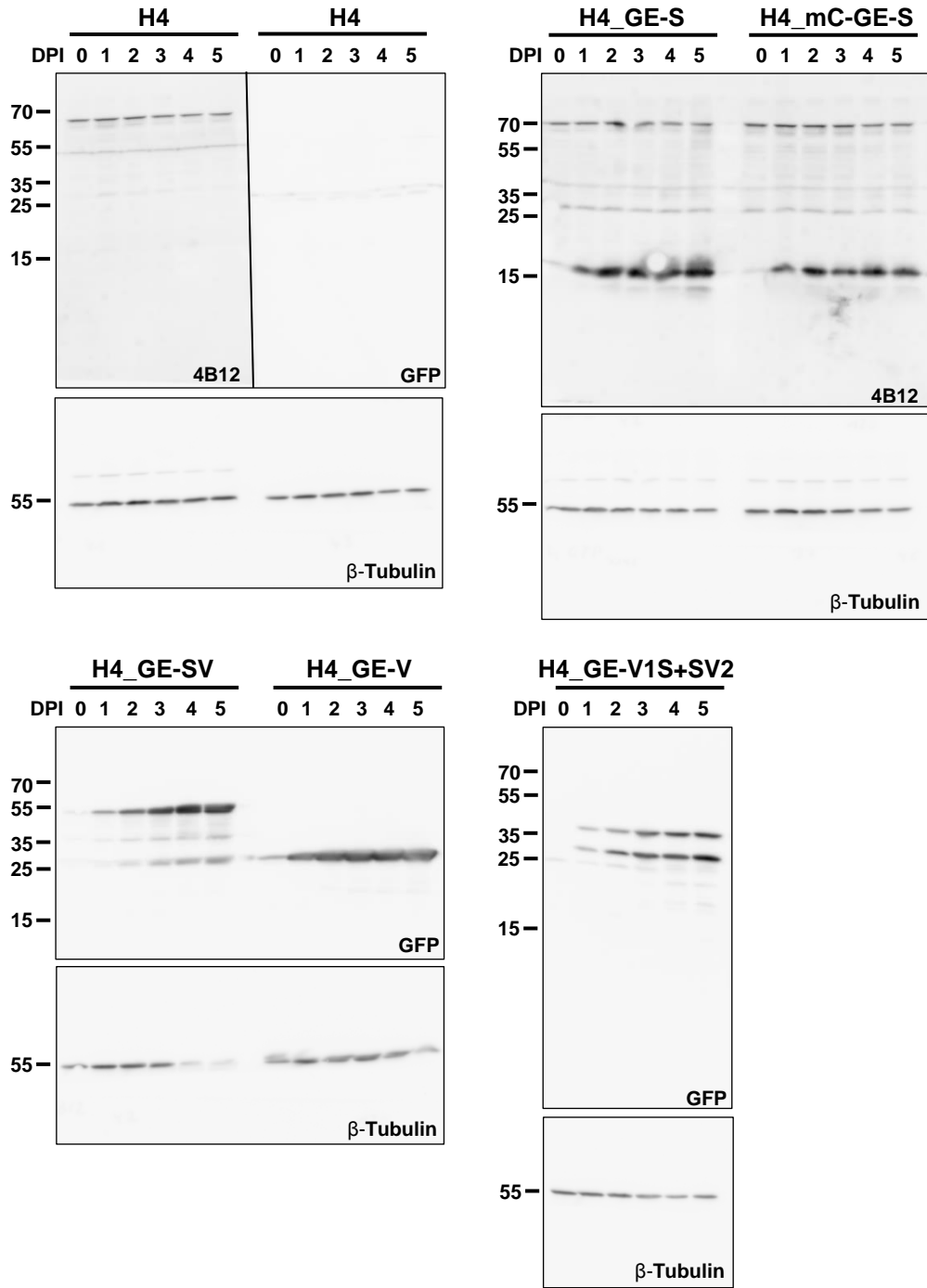
**Supplementary Figure 7.** Full length Western blots corresponding to the panels shown in Figure 5. For details see legend of Figure 5. All blots were stripped after incubated with 4B12 or GFP antibody and afterwards incubated with β-Tubulin antibody.
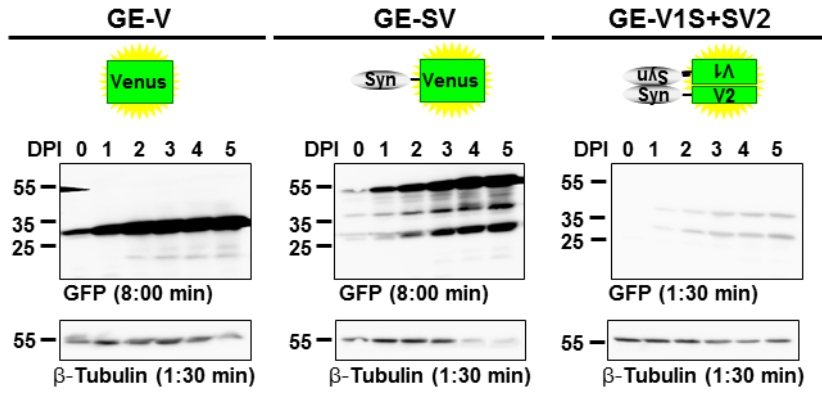
**Supplementary Figure 8.** Additional exposures of Western blots shown in Figure 5. For details see legend of Figure 5. All blots were stripped after incubation with GFP antibody and afterwards incubated with β-Tubulin antibody.
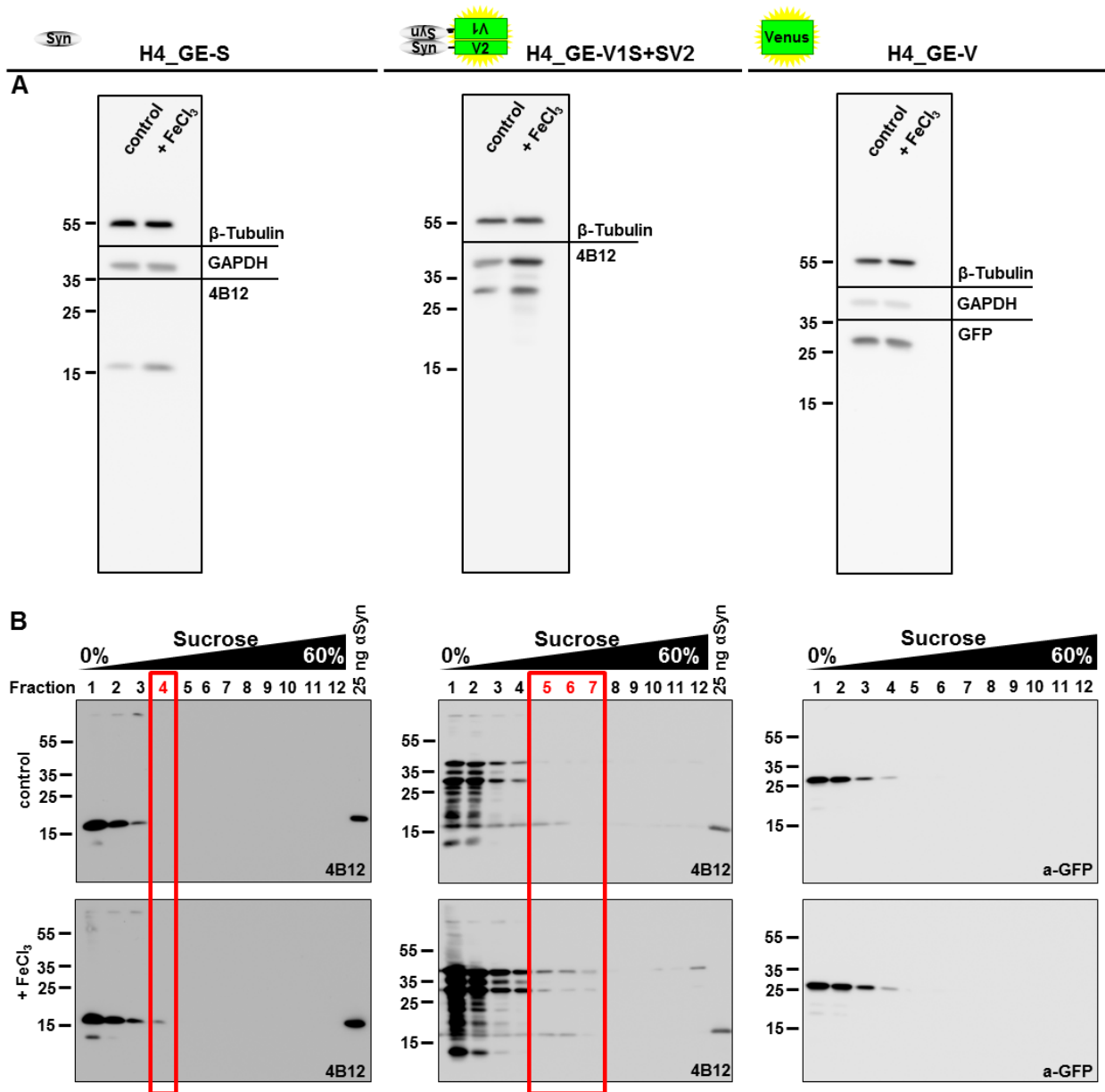
**Supplementary Figure 9.** (A) Full length Western blots corresponding to the panels shown in Figure 7 A. All blots were cut at 35 kDa and/or at 40 kDa and incubated with β-Tubulin, GAPDH, 4B12 or GFP antibody, respectively. (B) Full length Western blots corresponding to the panels shown in Figure 7 B. 25 ng of alpha-synuclein (αSyn) were loaded as control. For details see legend of Figure 7.
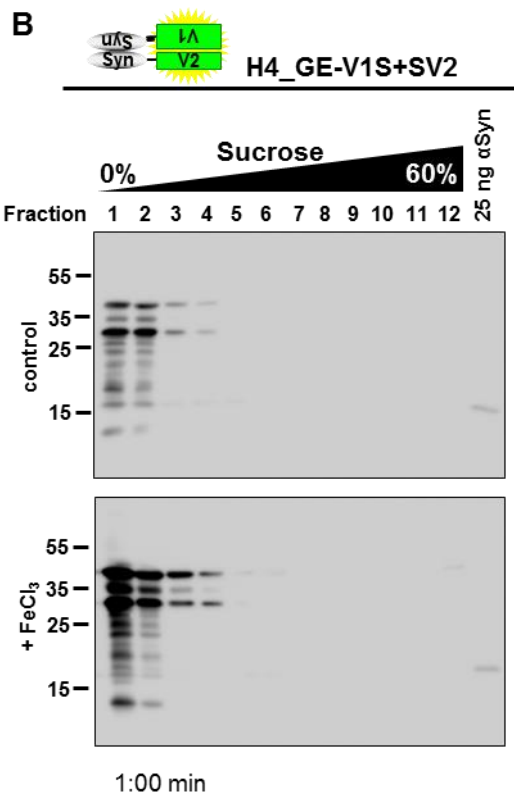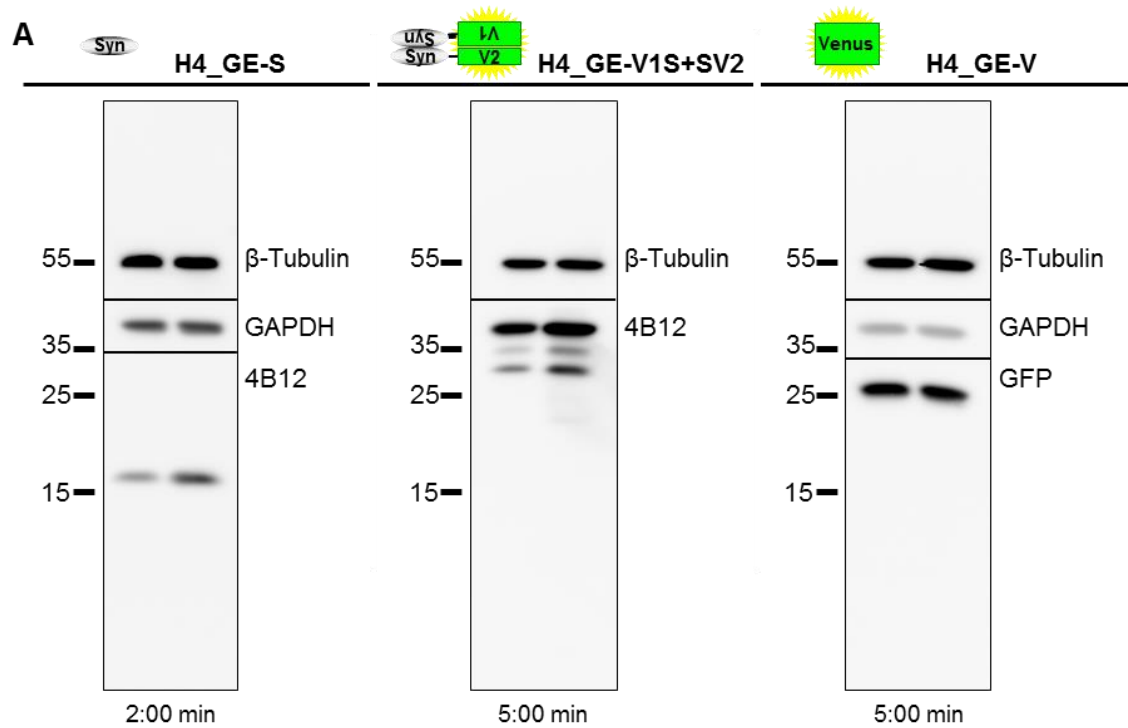
**Supplementary Figure 10.** Additional exposures of Western blots shown in Figure 7. All blots in (A) were cut at 35 kDa and/or at 40 kDa and incubated with β-Tubulin, GAPDH, 4B12 or GFP antibody, respectively. In (B), 25 ng of alpha-synuclein (αSyn) were loaded as control. For details see legend of Figure 7.

Supplementary Methods

## Measurement Setup of the Opera® System

Prior to measurement, nuclei were stained by incubating the cells for 15 min at 37°C in a humidified 95% air/5% $CO_2$ atmosphere with Draq5 (Thermo Fisher Scientific, 62252) diluted 1:1,000 in medium to a final concentration of 5 μM. High content screening was performed using the Opera® high-throughput confocal imaging platform (PerkinElmer Cellular Technologies GmbH, Hamburg, Germany). In this setup (Supplementary Figure 8 A), laser light can be emitted at four different wavelengths: 442 nm, 488 nm, 561 nm, and 640 nm. The light passes the Nipkow unit with the primary dichroic mirror depending on the filters and can be focused on the sample carrier using four different objectives: one 20-fold air objective (20x_Air_LUCPLFLN_NA=0.45), and three different water immersion objectives: 20xW_UAPO20xW3/340_NA=0.7, 40xW_PlanAPO_40xWLSM_NA=0.9, and 60xW_UPLAPO_60x_NA=1.2. Fluorescent dyes or proteins in the sample carrier will emit photons upon excitation by laser light with corresponding wavelengths. Since this fluorescence light is emitted in all directions, a part of it passes the objective and follows the way of the exciting laser light retrogradely until it is reflected by the primary dichroic mirror. Depending on its wavelength, fluorescence can finally be detected by three different cameras. Camera 3 can detect fluorescence excited with 640 nm. Fluorescence excited with all other lasers is mirrored at the detection dichroic mirror 2 ("Detection dichro 2") and subdivided according to its wavelength at the detection dichroic mirror ("Detection dichro"). Depending on the filter settings applied, light of given wavelengths is finally detected using Camera 1 or Camera 2.

In order to reduce background signal, the light in a conventional confocal fluorescence microscope would usually pass a pinhole which is inserted at a position corresponding to the intermediate image of a conventional optical microscope and would thus exclude signal from fluorescent particles below or above the focus plane. In the Opera® high-throughput confocal imaging platform the confocal pinholes are replaced by a Nipkow unit (Supplementary Figure 8 B). In this setup, the exciting laser light is focused by a microlense array before it passes the primary dichroic mirror, the pinhole disk, and the objective to finally excite fluorescent dyes or proteins in the sample. The fraction of fluorescence light that is guided retrogradely passes the pinhole disk, a spinning disk with holes arranged in an arched profile. The microlenses on the microlense array and the pinholes on the pinhole disk are arranged in a similar manner. Due to the rotation of the microlense array and the pinhole disk (with a speed of 25 revolutions per second) not a single point is detected but an arched area of the image. Due to the arrangement of the microlenses and the pinholes and the spinning of those disks, the single arched areas will add up to a complete image of the focal area.

The autofocus function enables a fully automated acquisition of fluorescence images. Here, characteristic reflections of the autofocus laser are detected when passing the bottom of the multiwell plate. Afterwards, laser light is focused on a defined height above the bottom of the multiwell plate depending on the desired image plane.

## Adjustment of the Opera® System

Prior to each experiment a reference image and a skew analysis have to be applied in order to compensate for systemic errors of the optics and the CCD cameras.

Uneven brightness distribution within an image was compensated for by using the "reference image" function. Using the Opera® adjustment plate, an image of free floating fluorescence dye was acquired. This should theoretically lead to evenly distributed fluorescence intensity within the image field. Practically, we observed higher intensity in the center of the image and decreasing intensity towards the

edges. This effect is counteracted by the flat-field correction algorithm which (simplified) works by multiplying the recorded image with the inverted reference image.

The mechanical alignment of the CCD cameras alone is subject to variations (for example due to changes in temperature) and not sufficient to provide an adequate overlay of high resolution images obtained from more than one camera. To counteract this phenomenon the "skew analysis" function was applied. The Opera® adjustment plate provides wells with beads with different diameters for the different objectives: 10 µm for 10-fold, 5 µm for 20-fold, and 2.5 µm for 40-fold and 60-fold. Images of these beads are recorded for all excitation wavelengths and all detection cameras. Afterwards, a theoretical optimal overlay of the obtained images is calculated. This optimization is later on applied to all images of one measurement.

In order to set up an automated experiment, the kind of multiwell plate and the required objective were defined. Wavelengths and intensities of laser light as well as corresponding filters were defined depending on experimental conditions. A "plate layout" (defining the wells of a multiwell plate) and a "sublayout" (defining the area insight the wells) where images should be acquired were defined.

All data from automated fluorescence imaging shown in this work have been acquired using the 20x air objective.


**Data Analysis using the Acapella® software**

An automated image analysis tool was developed in order to quantify cellular Venus fluorescence using the Acapella® software (PerkinElmer Cellular Technologies GmbH).

Here, nuclei (Supplementary Figure 12 A) and cell boundaries (Supplementary Figure 12 B) were automatically detected based on Draq5 signal. Based on this detection, an area for the quantification of mean cellular Venus fluorescence intensity was determined (Supplementary Figure 12 C). By setting an arbitrary threshold for the mean cellular Venus fluorescence intensity, cells were considered Venus-positive (Supplementary Figure 12 D) or Venus-negative (Supplementary Figure 12 E). As a final result, a table with high content data concerning different properties was obtained (Supplementary Figure 12 F).

**A**

Sample carrier

Objective lenses

Cam2

Cam3

LBC
(Laser excitation)

442 nm
488 nm
561 nm
640 nm

**Camera 2**
Filter changer

**Detection
dichro 2**

**Primary
dichro**

Power
meter

Cam1

**Detection
dichro**

Autofocus
laser

**Camera 1**
Filter changer

Nipkow unit

**B**

Microlense array

Pinhole disk

**Primary
dichro**

Laser light

Objective

Focal plane

Cam
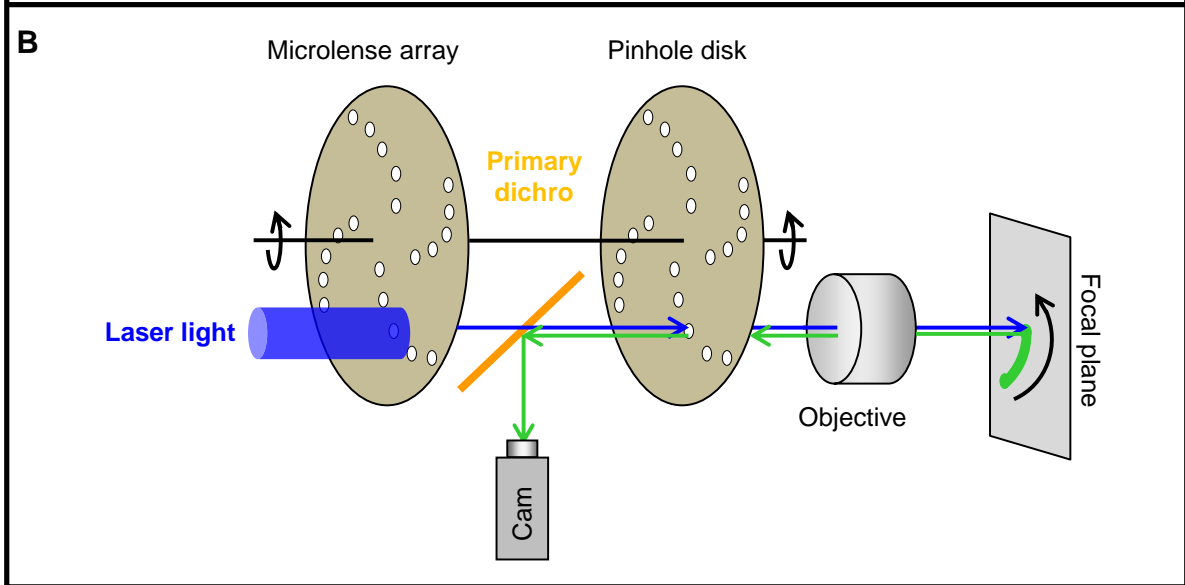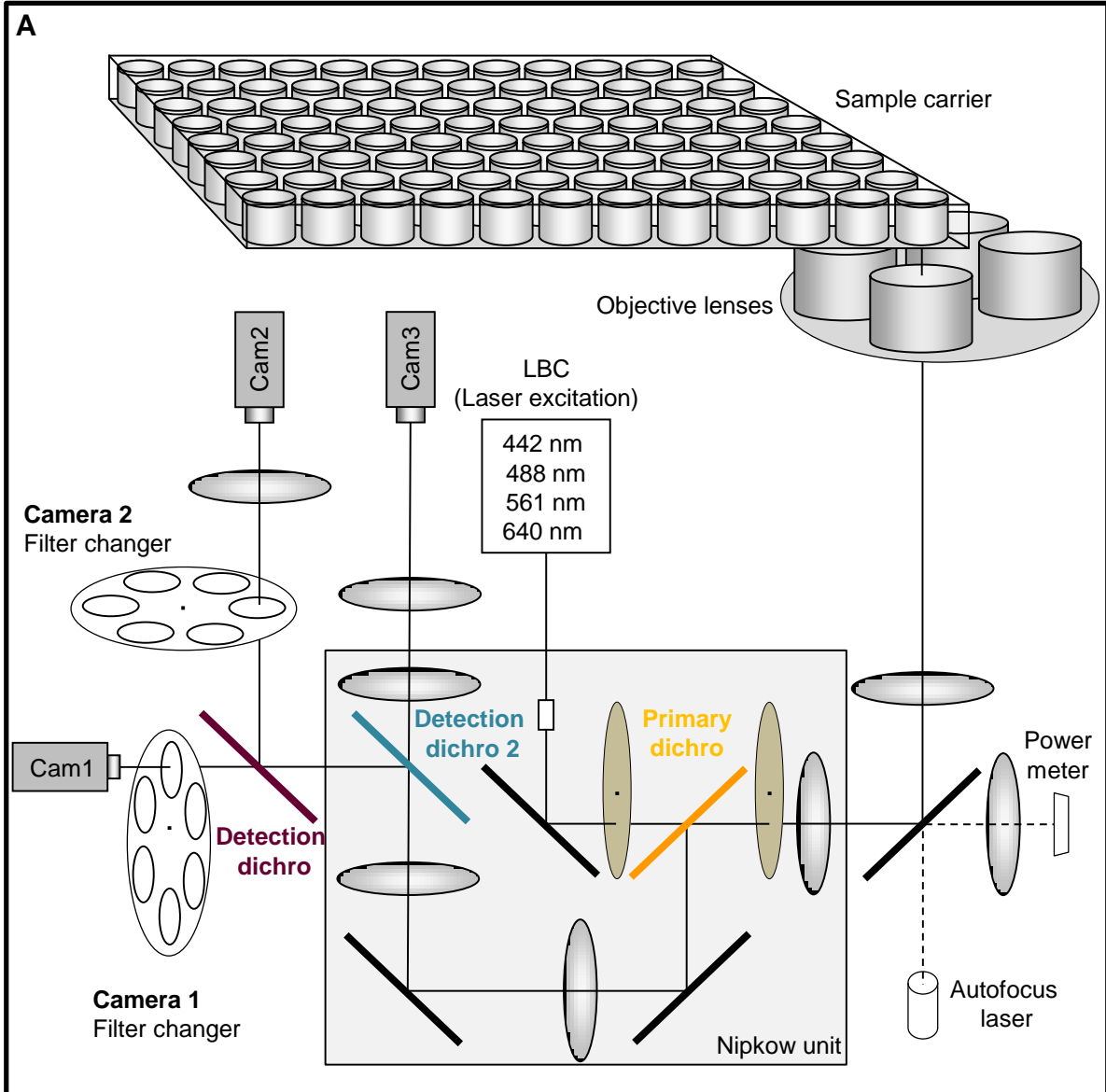
**Supplementary Figure 11. Measurement setup of the Opera®**

Schematic representation of the Opera® high-throughput confocal imaging platform and the Nipkow unit.

A) Laser light from four lasers (442 nm, 488 nm, 561 nm, and 640 nm) can be focused on the sample carrier via dichroic mirrors. Emitted photons pass the objective retrogradely and are guided via dichroic mirrors and a Nipkow unit to be detected separately using three different cameras.

B) The Nipkow disk inside the Nipkow unit consists of small holes arranged in an arched manner. Inside the Nipkow unit laser light is focused by microlenses in a disk with similar arrangement through the Nipkow disk and the objective on the sample. Emitted fluorescence is guided retrogradely through the Nipkow disk where the single holes decrease background fluorescence by excluding signals from above or below the focus plane. Due to the rotation of the Nipkow disk an arched image is recorded for each hole. The images of the different holes will finally add up to a complete image.
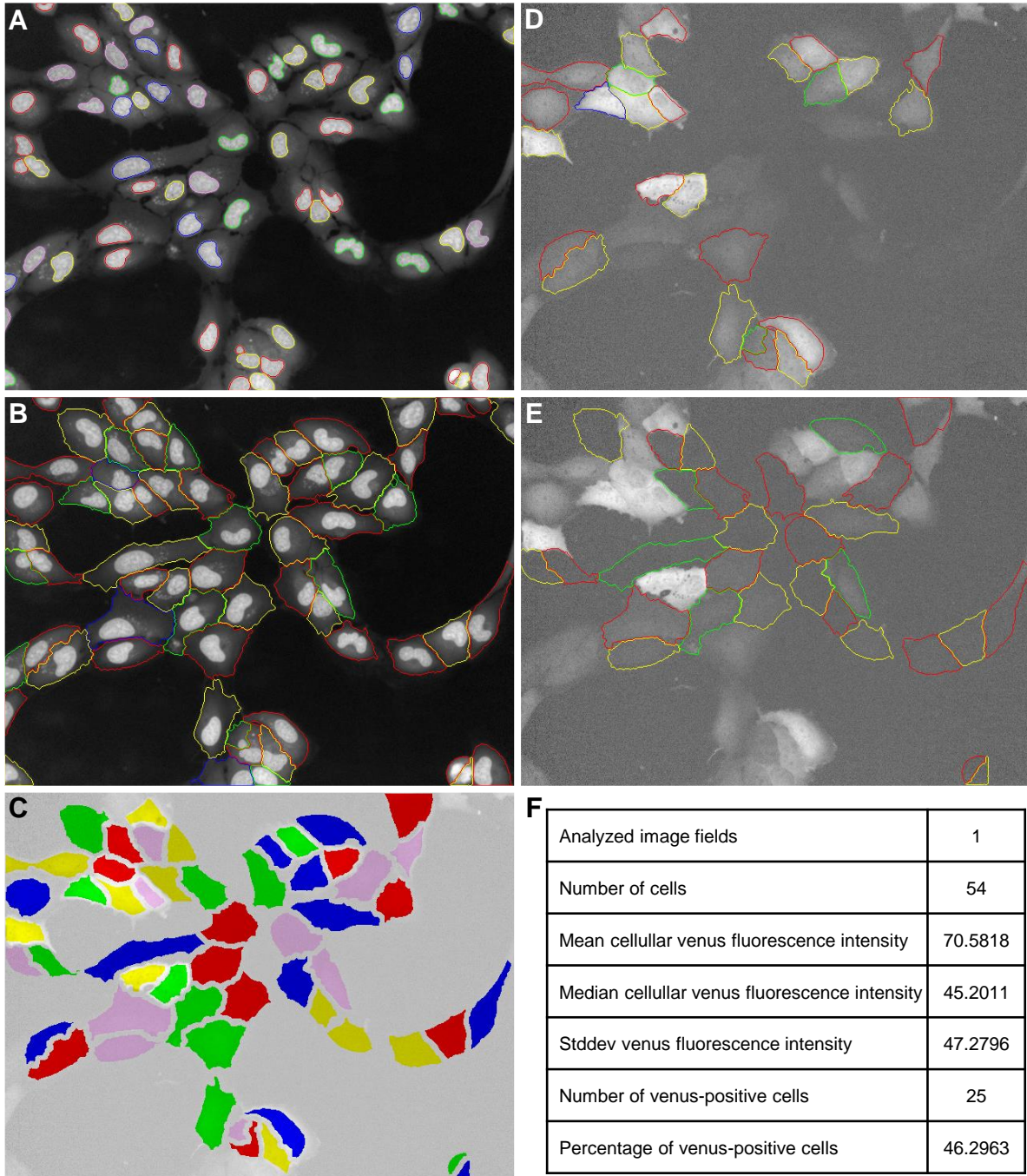
**Supplementary Figure 12. Acapella® data analysis**

Overview of the automated image analysis using the Acapella® software.

A) Detection of nuclei based on Draq5 fluorescence.
B) Determination of cell boundaries based on Draq5 fluorescence.
C) Definition of the area to quantify mean cellular Venus fluorescence.
D) Cells considered Venus-positive based on an arbitrarily set threshold for mean cellular Venus fluorescence.
E) Cells considered Venus-negative based on an arbitrarily set threshold for mean cellular Venus fluorescence.
F) Final output table showing different sample properties.